Expanding the One-Dimensional CdS–CdSe Composition Landscape: Axially Anisotropic $CdS_{1-x}Se_x$ Nanorods

T. Purnima A. Ruberu and Javier Vela*

Department of Chemistry, Iowa State University, and U.S. DOE Ames Laboratory, Ames, Iowa 50011, United States.

ABSTRACT We report the synthesis and characterization of $CdS_{1-x}Se_x$ nanorods with axial anisotropy. These nanorods were synthesized *via* single injection of a mixture of trioctylphosphine sulfur and selenium precursors to a cadmium–phosphonate complex at high temperature. Transmission electron microscopy shows nanoparticle morphology changes with relative sulfur and selenium loading. When the synthetic selenium loading is between 5% and 10% of total chalcogenides, the nanorods exhibit pronounced axial anisotropy characterized by a thick "head" and a thin "tail". The nanorods' band gap red shifts with increasing selenium loading. X-ray diffraction reveals that $CdS_{1-x}Se_x$ nanorods have a wurtzite crystal structure with a certain degree of alloying. High-resolution and energy-filtered transmission electron microscopy and energy-dispersive X-ray spectroscopy confirm the head of the anisotropic nanorods is rich in selenium, whereas the tail is rich in sulfur. Time evolution and mechanistic studies confirm the nanorods form by quick growth of the CdSe-rich head, followed by slow growth of the CdS-rich tail. Metal photodeposition reactions with 575 nm irradiation, which is mostly absorbed by the CdSe-rich segment, show effective electronic communication between the nanorod head and tail segments.

KEYWORDS: heterostructure · nanorod · axial anisotropy · graded alloy · cadmium chalcogenide

One-dimensional (1D) colloidal semiconductors (nanorods, nanowires) have been the subject of much recent interest.[1−7] For the particular case of cadmium chalcogenide nanorods, seminal papers have addressed their general synthesis,[8−14] nucleation and growth,[15] diameter and length control,[13,16] and morphology variants such as arrow-, teardrop-, and branched (tetra- and multipod)-shaped nanocrystals.[17,18] Significant attention has been paid to the microscopic mechanism of uncatalyzed anisotropic growth of cadmium chalcogenide nanorods *via* hot injection methods. At low precursor concentrations, surface area minimization *via* Ostwald ripening favors formation of spherically shaped (0D) colloidal nanocrystals (dots). However, typical nanorod preparations use cadmium oxide (CdO) and a bulky phosphonic acid such as octadecyl phosphonic acid (ODPA). The resulting cadmium–phosphonic acid complex is very stable and serves as a slow, controlled source of cadmium ions, which helps maintain a high precursor concentration.[19] At high precursor concentrations, the relative growth rates of different crystallographic facets play a major role in determining the final shape of the nanocrystals.[17,20] This is particularly important for wurtzite-type cadmium chalcogenides, which are intrinsically anisotropic materials with a unique *c* axis.[15,21] Two possible facets perpendicular to the wurtzite *c* axis are 001 and $00\bar{1}$ facets, which terminate respectively on positively charged Cd and negatively charged Se ions. Various studies have proven the $00\bar{1}$ facet has the highest growth rate of all facets.[17,21] These Se-rich $00\bar{1}$ facets are relatively uncoated because ligands in solution are usually electron donating. In addition, the permanent dipole moment along the unique *c* axis enhances the chemical potential of the $00\bar{1}$ facet.[22,23] The unique structural features of the $00\bar{1}$ facet favor unidirectional growth on this facet, that is, along the *c* axis.[24]

Continued research on synthesis of colloidal nanocrystals is quickly moving toward new preparative methods of increased power and complexity. Of particular interest is finding new ways to produce heterostructured and highly anisotropic nanocrystals—those made up by two or more distinct phases and containing very large aspect ratios and/or different shapes—that could be assembled into functional materials and devices. In the case of cadmium chalcogenide nanocrystals, different groups have reported syntheses for spherical (0D) alloyed $CdS_{1-x}Se_x$,[25−28] $CdSe_xTe_{1-x}$,[29] and $Cd_{1-x}Hg_xTe$[30] quantum dots, core/shell CdSe/CdS,[31−34] CdTe/CdS,[35,36] CdSe/ZnS,[37−40] and CdSe/ZnSe[41] quantum dots, multishell $CdS/Zn_{0.5}Cd_{0.5}S/ZnS$

* Address correspondence to vela@iastate.edu.

Received for review April 20, 2011 and accepted June 2, 2011.

Published online June 02, 2011
10.1021/nn201466b

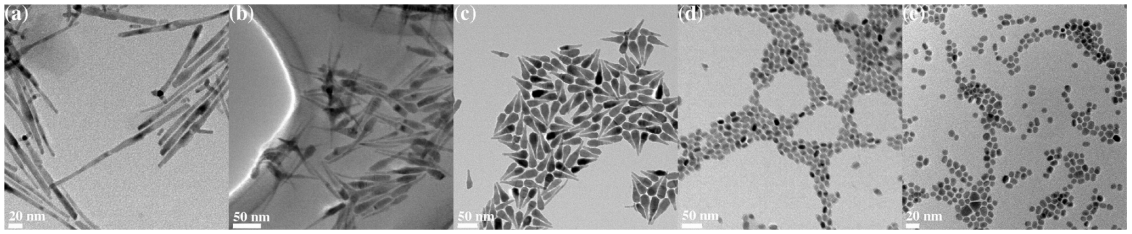

Figure 1. TEM micrographs showing $CdS_{1-x}Se_x$ morphology as a function of Se loading (actual EA composition in parentheses): (a) 0% Se loading (CdS), (b) 5% Se loading ($CdS_{0.68}Se_{0.32}$), (c) 10% Se loading ($CdS_{0.42}Se_{0.58}$), (d) 20% Se loading ($CdS_{0.33}Se_{0.67}$), (e) 100% Se loading (CdSe). Scale bars: 20 nm (a, e), 50 nm (b, c, d).

TABLE 1. Composition and Dimensions of Axially Anisotropic $CdS_{1-x}Se_x$ Nanorods

entry	rxn time/min	%Se loading[a]	%Se composition: EA[b] (XRD)[c]	total length/nm (XRD)[d]	head diameter/nm	tail diameter/nm	aspect ratio[e]
1	85	0	0[b] (0)[c]	154.1 ± 30.4 (43.0)[d]	5.6 ± 0.8	5.6 ± 0.8	27
2	85	5	32[b] (45)[c]	91.3 ± 6.4 (24.0)[d]	12.8 ± 1.9	3.7 ± 0.4	7.0
3	85	10	58[b] (63)[c]	59.3 ± 8.0 (29.1)[d]	17.8 ± 2.4	5.6 ± 0.8	3.3
4	85	20	67[b] (81)[c]	20.5 ± 2.9 (13.4)[d]	11.8 ± 1.7	11.8 ± 1.7	1.7
5	85	100	100[b] (100)[c]	11.4 ± 2.1 (10.5)[d]	8.5 ± 1.0	8.5 ± 1.0	1.3
6[g]	20	5	n.d.[f] (n.d.)[f]	51.8 ± 5.4[g] (n.d.)[f]	14.0 ± 1.1[g]	14.0 ± 1.1[g]	3.7
7[h]	85	—[h]	n.d.[f] (n.d.)[f]	37.5 ± 7.4 (n.d.)[f]	10.2 ± 1.1	3.7 ± 0.6	3.7

[a] %Se used during synthesis. [b] Determined by elemental analysis. [c] Estimated from XRD. [d] Calculated from (002) peak. [e] Minimum aspect ratio = length/head diameter. [f] Not determined. [g] Also observed small dots with a diameter = 3.1 ± 0.8 (see Figure 8a). [h] Made in the presence of premade, pure CdSe nanorods, using a 0% Se loading.

quantum dots,[42] and one-dimensional (1D) core/shell CdSe/CdS and CdSe/ZnS nanorods,[43−46] CdSe−CdTe segmented nanorods,[47−49] alloyed CdHgTe nanorods,[50] alloyed $CdS_{1-x}Se_x$ nanowires,[51] coaxial core/shell Si/CdSSe nanowires,[52] segmented CdS−CdSe[53] and CdSe−ZnSe[54] nanowires, seeded CdSe−CdS,[45] CdTe−CdSe,[55] and $CdSe_xTe_{1-x}$ rods[56] and tetrapods,[57] CdS−Ag_2S nanorod superlattices,[9] and CdSSe nanoribbons.[58,59] There is also increasing interest in cadmium chalcogenide−metal hybrid nanomaterials,[60−63] including CdS, CdSe, and CdSe/CdS nanorods bound to PbSe,[64] Fe_2O_3,[65,66] Bi,[54] Fe−Pt,[67] Au,[68,69] Pt,[70−73] Pd,[74] and Co nanoparticles.[75,76]

In this paper, we report the synthesis of axially anisotropic, colloidal $CdS_{1-x}Se_x$ nanorods that are characterized by having distinct thick and thin ends. These nanocrystals form spontaneously over relatively long reaction periods (∼1.4 h) when a mixture of trioctyl phosphine sulfide and selenide (TOPS and TOPSe) is used as chalcogenide source, specifically with TOPS to TOPSe ratios between 95:5 and 9:1. Using a combination of optical and structural characterization methods, we show the amount of Se in these nanorods is much higher (up to 6×) than what could be expected from TOPSe loading used during their synthesis. We also show axially anisotropic $CdS_{1-x}Se_x$ nanorods are single crystalline, with an axial composition gradient between a CdSe-rich thick end and a CdS-rich thin end. Using different control experiments, we explore the mechanism of formation of these axially anisotropic nanorods and establish that they form in a sequential manner, where quick growth of a CdSe-rich head (≤20 min) precedes slow growth of a CdS-rich tail (∼85 min). Finally, we probe the degree of electronic communication between the two segments of the nanorods by carrying out palladium photodeposition experiments. We show palladium photodeposition occurs along the whole length of the nanorods using a lamp whose light is absorbed by the smaller band gap CdSe-rich segment, but not by the larger band gap CdS-rich segment.

RESULTS AND DISCUSSION

As part of a study directed at harvesting sunlight with one-dimensional semiconductor colloids, we became interested in CdSe based on its relatively small band gap (1.7 eV bulk). However, we faced difficulties in making CdSe nanorods and frequently obtained instead mixtures of CdSe dots, rods, and multipods. While we amply recognize these complications arise from variable amounts of impurities present in different batches of chemicals, removing such impurities by purification added unwanted and lengthy extra steps to our synthesis. In contrast, we noted that a procedure recently reported for making CdS nanorods is highly reproducible, even without prior purification of precursors or ligands.[9] This procedure involves reaction between trioctylphosphine sulfide and an *in situ*-generated cadmium−octadecyl phosphonate complex in trioctylphosphine oxide at 315 °C for 85 min and results in long (154.1 ± 30.4 nm) and thin (5.6 ± 0.8 nm diameter) CdS nanorods with a high aspect ratio (length/diameter) of 27 and a small size dispersion (Figure 1a and entry 1 in Table 1). Unfortunately, CdS is a bluer, larger band gap (2.4 eV bulk) material compared to CdSe and is less attractive for harvesting

sunlight. Nonetheless, we reasoned that introducing small amounts of Se during synthesis might lead to $CdS_{1-x}Se_x$ nanorods with a smaller band gap compared to pure CdS.

$CdS_{1-x}Se_x$ Nanorod Morphology. To test this idea, we replaced TOPS in the injection solution with a mixture of TOPS and TOPSe while keeping the total chalcogenide concentration constant. To our surprise, not only does replacing a fraction of TOPS with TOPSe lead to $CdS_{1-x}Se_x$ nanorods, but such $CdS_{1-x}Se_x$ nanorods can display a high degree of anisotropy along their main axis when the total amount of chalcogenides contains 10% or less Se loading. Figure 1 shows the morphology of $CdS_{1-x}Se_x$ nanocrystals that result from changing Se loading in each preparation. Figure 2 shows the corresponding changes in $CdS_{1-x}Se_x$ nanorod length, diameter, and aspect ratio as a function of Se loading. These trends are quantitatively summarized in Table 1.

At 0% Se loading, long nanorods form with a consistent diameter of 5.6 ± 0.8 nm along their whole length (Figure 1a and entry 1 in Table 1). Increasing Se loading between 1% and 10% leads to axially anisotropic nanorods having two distinct fat (head) and thin (tail) ends (Figure 2b). For example, at 5% Se loading the nanorods have head and tail diameters of 12.8 ± 1.9 and 3.7 ± 0.4 nm, respectively, whereas at 10% Se loading the nanorods have head and tail diameters of 59.3 ± 8.0 and 17.8 ± 2.4 nm, respectively. We casually referred to these nanocrystals as having "tadpole" (5% Se) or "drumstick" (10% Se) morphology (Figure 1b,c and entries 2 and 3 in Table 1). Qualitatively, these tadpole and drumstick $CdS_{1-x}Se_x$ nanocrystals appear to have similar morphology to "paddle" CdS and "teardrop" CdSe nanocrystals previously reported in the literature.[13,17] Increasing Se loading above 10% Se leads to progressively shorter nanorods that once again retain a consistent diameter along their length (Figure 2b). For example, at 20% Se loading nanorods have a consistent diameter of 11.8 ± 1.7 nm (Figure 1d, e and entries 4 and 5 in Table 1). Across the $CdS_{1-x}Se_x$ series, the nanorods' length dramatically decreases from 154.1 ± 30.4 nm to 11.4 ± 2.1 nm for 0% and 100% Se loading, respectively (Figure 2a).

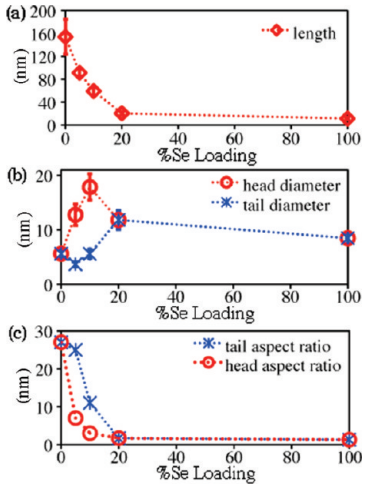

Figure 2. Effect of %Se loading on $CdS_{1-x}Se_x$ length (a), diameter (b), and aspect ratio (c).

Optical Properties of $CdS_{1-x}Se_x$ Nanorods. As initially expected, the absorption spectrum of $CdS_{1-x}Se_x$ nanorods is red shifted compared to pure CdS nanorods. Figure 3a shows that the absorption edge of $CdS_{1-x}Se_x$ nanorods shifts to longer wavelengths as Se loading increases, and Figure 3b shows the corresponding change in apparent band gap (estimated from first absorption peak). As shown in Figure 3b, even a modest increase in Se loading, from 0% to 5% Se, causes a dramatic drop in apparent band gap. This strongly indicates the concentration of Se in these nanocrystals is much higher than calculated based on synthetic Se loading alone (see further discussion below). The photoluminescence properties of $CdS_{1-x}Se_x$ nanorods also change depending on the amount of Se present, and the observed changes are compounded by the nanorods' complex composition and structure (presented below). Qualitatively, Figure 3c and d show preparations where using Se loadings between 10% and 100% result in weakly luminescent nanorods, with

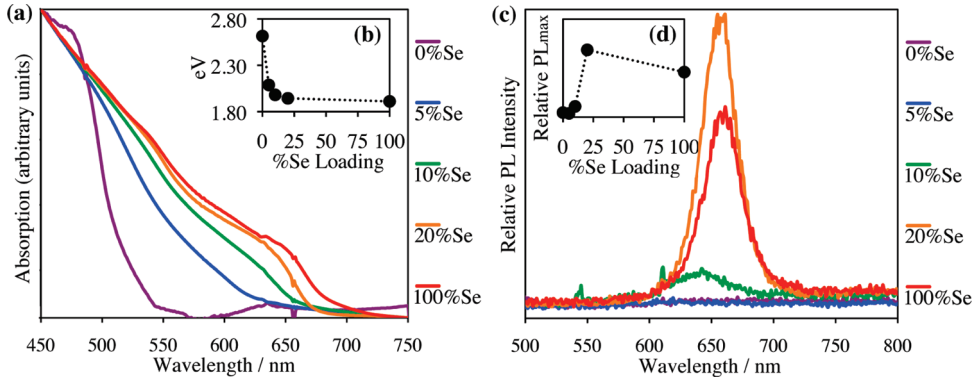

Figure 3. $CdS_{1-x}Se_x$ optical properties: Change in absorption (a), band gap (b), and PL intensity (c, d) with increasing Se loading. (Low solubility of CdS nanorods results in scattering above 500 nm.)

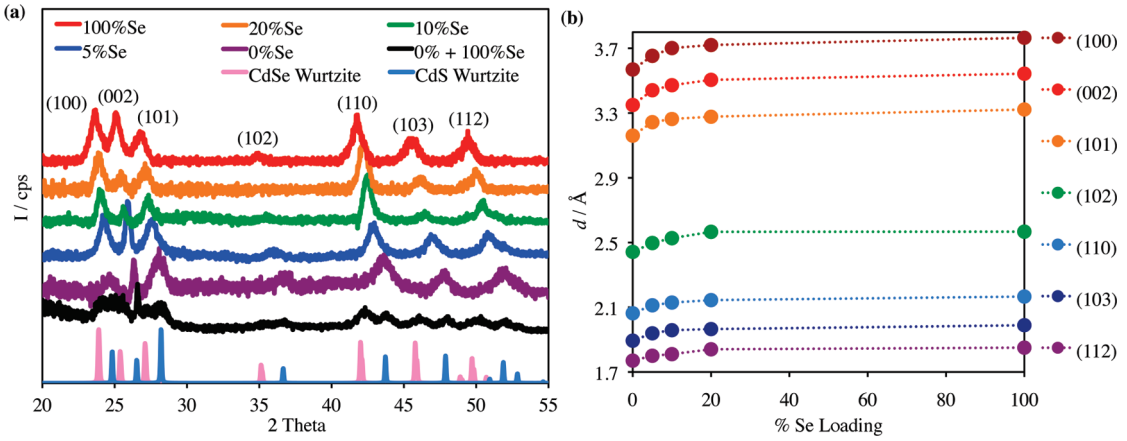

Figure 4. (a) $CdS_{1-x}Se_x$ XRD patterns for different %Se loadings. XRD patterns of a pure CdS/pure CdSe mixture. The 0% + 100% Se loading and bulk wurtzite (hexagonal) CdSe and CdS are shown for comparison. (b) Change in $CdS_{1-x}Se_x$ interplanar *d*-spacings as a function of %Se loading.

maximum relative luminescence (QY ≈ 0.2%) corresponding to nanorods obtained with a 20% Se loading.

$CdS_{1-x}Se_x$ Nanorod Structure and Overall Composition. Figure 4a shows powder X-ray diffraction patterns of several $CdS_{1-x}Se_x$ nanorod samples with different Se loadings. Each XRD pattern consists of a single set of peaks most consistent with a hexagonal, wurtzite crystal structure. We can rule out the presence of two separate pure CdS and CdSe phases in these samples on the basis of the fact that each $CdS_{1-x}Se_x$ XRD pattern consists of a single set of peaks (Figure 4a). A control sample made by mixing pure CdS and CdSe nanorods (0% Se and 100% Se) has an XRD pattern that consists of two distinct sets of peaks, with two peaks showing for each set of lattice planes (Figure 4a). In contrast, all $CdS_{1-x}Se_x$ nanorod samples with $1 > x > 0$ show a single peak for each set of lattice planes, and individual 2·theta (2θ) values fall in between the values for pure wurtzite CdS and CdSe phases reported in the Inorganic Crystal Structure Database (ICSD 2010-2/2010 from Fachinformationszentrum Karlsruhe (FIZ) and NIST FindIt Version 1.7.1.). Individual diffraction peaks progressively shift to smaller 2θ values (wider *d*-spacings) with increasing Se loading, in agreement with lattice expansion to accommodate the incorporation of increasing amounts of larger Se ions. This indicates some type of alloying between CdS and CdSe phases in these nanostructures. To investigate this further, we plotted the experimentally measured *d*-spacings for each set of lattice planes as a function of Se loading. Figure 4b shows such plot is nonlinear but highly curved, which is typical of non-Vegard behavior.[77] This observation strongly indicates that the nanocrystals may not be completely alloyed, but instead contain some degree of heterostructuring, perhaps in the form of a graded alloy. Note: A homogeneous alloy or solid solution could have formed based on relative S^{2-} (1.7 Å) and Se^{2-} (1.84 Å) ionic sizes (8.2% difference) and CdSe (7.010 Å) and CdS (6.749 Å) wurtzite lattice paramaters (3.9% lattice mismatch).

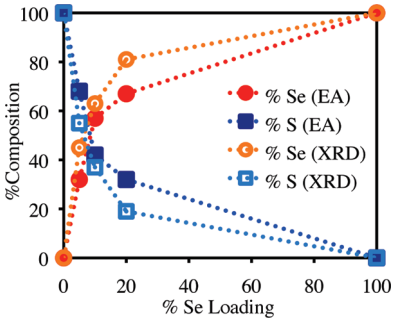

Figure 5. $CdS_{1-x}Se_x$ composition obtained experimentally from elemental analysis and X-ray diffraction plotted against synthetic Se loading.

Another feature observed from powder diffraction data is that the length of the nanorods calculated from the (002) X-ray diffraction (XRD) peak is almost always shorter than that measured from transmission electron microscopy (TEM) (Table 1). This behavior has been previously observed and attributed to the presence of stacking faults along the nanorods' length, which effectively decreases the apparent nanocrystal size.[17] Figure 4b also shows that individual XRD peaks occur at smaller 2θ values and correspond to larger *d*-spacings than could be expected from Se loadings used in the synthesis. Figure 5 shows the actual composition of $CdS_{1-x}Se_x$ nanorods obtained from experimental XRD data as well as from chemical elemental analysis (EA). Both XRD and EA data confirm that the nanorods' actual Se content is always higher than the Se loading used during their synthesis, which strongly indicates Se has a higher tendency than S to incorporate into these nanostructures. By comparing experimental XRD and EA data with the corresponding Se loadings (Table 1), we estimate there is a 3- to 9-fold (3−9×) preference for Se over S to go into these nanostructures.

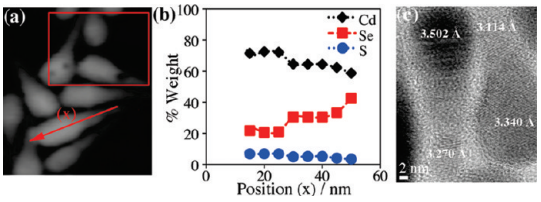

Figure 6. Individual $CdS_{0.42}Se_{0.58}$ nanorod sample analyses: (a) Direction and length (*x*) and (b) composition plot of an EDS line scan (arrow length = 50 nm; square area was used for drift correction). (c) HR-TEM micrograph showing interplanar (002) *d*-spacings (perpendicular to *c* axis) become progressively larger from the tail to the head of the nanorods.

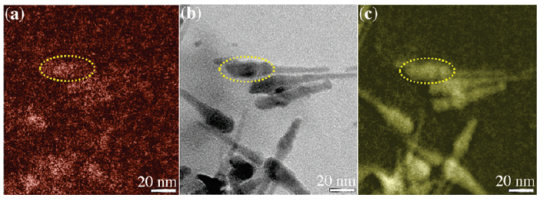

Figure 7. Registered EF-TEM images of tadpole-like $CdS_{0.68}Se_{0.32}$nanorods: (a) Se-channel, (b) regular TEM, and (c) S-channel.

S and Se Atom Distribution in $CdS_{1-x}Se_x$ Nanorods. The unusual anisotropic morphology observed by TEM suggests $CdS_{1-x}Se_x$ nanorods possess an inhomogeneous composition along their length.[25] To answer this question, we resorted to high-resolution (HR)-TEM, energy dispersive X-ray spectroscopy (EDS), and energy-filtered (EF)-TEM. Figure 6 shows representative EDS and HR-TEM data of drumstick-like $CdS_{0.42}Se_{0.58}$ nanorods that result from 10% Se loading. EDS line scans along the nanorods' main axis show that Se content dramatically increases on going from tail to head regions (Figure 6a,b). HR-TEM confirms nanorods are single crystalline, as judged by the continuity in lattice fringes along their structure (Figure 6b). We also used HR-TEM to measure interplanar *d*-spacings at different points along the length of several of these nanorods and found the *d*-spacings get consistently larger on going from the tail to head regions. This can be attributed to a higher fraction of larger Se atoms at the head and a higher fraction of smaller S atoms at the tail of the nanorods. The net result of this composition gradient is lattice expansion toward the head of the nanorods.

Figure 7 shows three registered TEM and EF-TEM images of tadpole-like $CdS_{0.68}Se_{0.32}$ nanorods that result from 5% Se loading. In agreement with what is observed by EDS and HR-TEM on the shorter nanorods, Se-channel EF-TEM indicates Se is preferentially located at the thicker head region of the nanorods (Figure 7a *vs* b), whereas the S-channel EF-TEM image indicates S distributes along the whole length of the nanorods (Figure 7c *vs* b). Taken together, these EDS, HR-TEM, and EF-TEM results unambiguously confirm Se incorporates preferentially at the head region of the nanorods, whereas mostly S is present at the tail region of the nanorods. The structural and single-crystalline continuity of the nanorods along their axis, along with progressively increasing Se concentration toward their head, is consistent with these structures being graded alloys.

Formation Mechanism of Anisotropic $CdS_{1-x}Se_x$ Nanorods. Having established the heterostructured, graded-alloy composition of anisotropic $CdS_{1-x}Se_x$ nanorods, we turned our attention to their growth mechanism. Our most immediate question was whether CdSe-rich (head) and CdS-rich (tail) segments formed (a) concomitantly (that is, both segments form in parallel simultaneously), (b) sequentially (one segment forms first, the other forms from it), or (c) independently of each other.

To probe this question, we studied time evolution of particles by stopping the reaction and characterizing products at different times. Figure 8a–c shows key results from such experiments using $CdS_{0.68}Se_{0.32}$ nanorods obtained with a 5% Se loading as a model system. At relatively short reaction times, for example after 20 min, we observed formation of thick nanorods (51.8 ± 5.4 nm in length, 14.0 ± 1.1 nm in diameter) along with a few small dots (3.1 ± 0.8 nm) (Figure 8a and entry 6 in Table 1). However, after 85 min thick nanorods appeared to grow a thin tail and produced tadpole-like, final anisotropic nanorods (91.3 ± 6.4 nm in length), small dots disappeared (Figure 8b and entry 2 in Table 1). Interestingly, the diameter of the 20 min nanorods (14.0 ± 1.1 nm) and head diameter of the 85 min nanorods (12.8 ± 1.9 nm) are the same within experimental error, strongly suggesting both share the CdSe-rich composition described above. Formation of a few small dots and their eventual disappearance along with formation of long nanorod tails is consistent with initial formation of CdS homonuclei, which dissolve over time in favor of heterogeneous nucleation on one side of the thick CdSe nanorods along the *c* axis, perpendicular to the (002) set of planes. To confirm these results, we repeated the procedure used to make pure CdS nanorods (using only TOPS or with a 0% Se loading) in the presence of pure CdSe nanorods (premade using only TOPSe or with a 100% Se loading) (Figure 8d–f). In the absence of CdSe nanorods, pure and long CdS nanorods are formed, as shown previously (see above).[9] However, in the presence of CdSe nanorods, these acted like seeds for formation of highly anisotropic, drumstick-like $CdS_{1-x}Se_x$ nanorods (Figure 8e), in agreement with the time-dependent mechanistic experiment above.

We then attempted to form anisotropic nanorods from preformed CdS nanorods by reacting pure CdS nanorods with TOPSe (Figure 8g–i). This experiment was unsuccessful, in that the length (188.3 ± 53.4 nm), diameter (9.1 ± 4.6 nm), and overall aspect of the initial CdS nanorods remained constant within experimental error. Some etching of the CdS nanorod surface occurred, however, as judged by formation of a few medium-size dots consistent with formation of CdSe

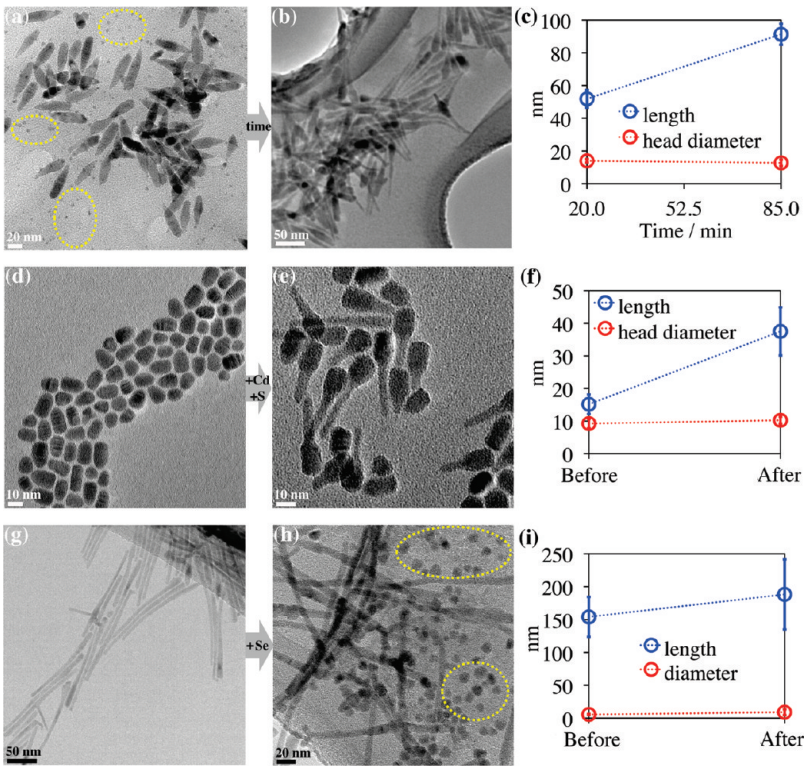

Figure 8. Mechanistic investigations of anisotropic $CdS_{1-x}Se_x$ nanorod formation. (a−c) Time evolution of $CdS_{0.68}Se_{0.32}$ nanorods: At short reaction times (20 min), the nanorod's head has already formed, along with very small CdS nuclei (circled) (a). Over time (85 min total reaction time), small CdS nuclei dissolved and only final $CdS_{0.68}Se_{0.32}$ nanorods were observed. (d−i) Independent formation of $CdS_{1-x}Se_x$ nanorods from preassembled elements. (d−f) Reaction of CdSe nanorods (d) with Cd and S precursors results in $CdS_{1-x}Se_x$ nanorod formation (e), (g−i) whereas reaction of CdS nanorods (g) with Se does not (a few CdSe nuclei, circled, formed instead) (h).

(10.8 ± 2.6 nm) (Figure 8h). Additional experiments where we treated CdS nanorods with both TOPSe and Cd−phosphonate precursors were similarly unsuccessful, leading to rectangular block-shaped nanocrystals with dimensions (65.2 ± 8.8 nm) × (18.7 ± 3.8 nm) instead of axially anisotropic nanorods (not shown). Together, these results demonstrate that while thin CdS tails can form starting from fat CdSe nanorod seeds, the opposite cannot happen; namely, fat CdSe heads cannot form from thin CdS tail seeds. In other words, formation of heterostructured, graded-alloy anisotropic $CdS_{1-x}Se_x$ nanorods is a sequential process that starts by quick growth of a CdSe-rich nanorod head, followed by slow growth of a CdS-rich tail.

Perhaps an even more intriguing question is the reason behind sequential formation of axially anisotropic $CdS_{1-x}Se_x$ nanorods. It is clear from our observations that under the experimental conditions used in this study the rate of CdSe nanorod (head) growth (≤20 min) is much faster than the rate of CdS nanorod (tail) growth (~85 min). The relative ease of formation of these nanorods cannot be a consequence of relative thermodynamics of crystalline energies, since CdS is a much more stable crystalline system compared to CdSe. On the basis of literature thermochemical data,[78] we calculate the lattice energy of CdS, 834 kcal/mol, is significantly higher than that for CdSe, 798 kcal/mol. These values are consistent with the melting points of CdS, 1748 °C, and CdSe, 1512 °C. Instead, we believe the relative ease of formation of nanorods is a consequence of relative reactivity of TOPS and TOPSe in solution. For tertiary alkyl phosphines such as TOP, the strength of a terminal P−Se bond is 75 kcal/mol, whereas the strength of a terminal P−S bond is 96 kcal/mol.[79] Because of the significantly weaker P−chalcogen bond strength in TOPSe compared to TOPS, by 21 kcal/mol, one can expect TOPSe to be much more reactive toward the Cd−phosphonate precursor than TOPS, leading to faster formation of CdSe compared to CdS. This suggests it may be possible to control relative degrees of Se and S in these and other nanostructures by judicious control of molecular precursors,[25] but further work is needed to confirm this idea.

Electronic Communication among CdSe- and CdS-Rich Segments. A key feature sought for many potential applications of heterostructured nanomaterials is good optical and electronic communication between the heterostructure's different components. To probe this aspect, we carried out photodeposition of palladium nanoparticles on axially anisotropic $CdS_{1-x}Se_x$ nanorods (Figure 9). Others[60−76] and we (to be communicated) have independently observed that photodeposition of metals on the surface of colloidal semiconductor nanocrystals can be selectively carried out using lasers or

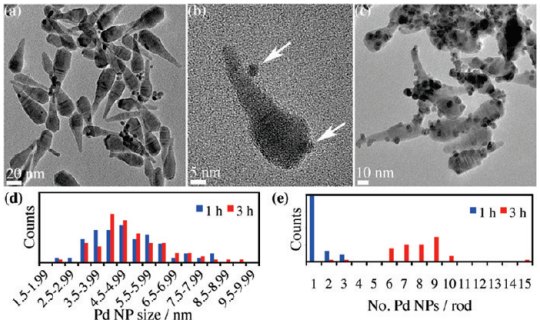

Figure 9. Photodeposition of Pd nanoparticles on $CdS_{0.42}Se_{0.58}$ nanorods obtained with a 10% Se loading: (a, b) 575 nm lamp, 1 h irradiation; (c) 575 nm lamp, 3 h. (The arrows in b point to Pd particles on tail and head segments.) (d) Pd nanoparticle size histogram. (e) Pd nanoparticle count per nanorod histogram. (Size measurements and statistics were obtained for at least 50−100 particles.)

fluorescent lamps. Light absorption by the semiconductor results in formation of electron−hole pairs that can be subsequently quenched by surface defect or "trap" states. The resulting surface-localized electrons can serve as reduction and seeding points for formation of metal nanoparticles from soluble organometallic precursors. Here, we used a 575 nm lamp (~75 nm fwhm) and (TMEDA)$PdMe_2$ to deposit Pd on $CdS_{0.42}Se_{0.58}$ nanorods obtained with a 10% Se loading (Figure 9). After 1 h irradiation, Pd nanoparticles formed having a size of 5.0 ± 1.5 nm, with an average of 1.3 Pd particles per nanorod and a maximum of 3 Pd particles per nanorod. After 3 h irradiation, Pd nanoparticles formed having a size of 5.1 ± 1.4 nm, with an average of 8.0 Pd particles per nanorod and a maximum of 15 Pd particles per nanorod (Figure 9). Clearly, irradiation time does not impact Pd nanoparticle size; however Pd loading greatly increases with longer irradiation times, as evidenced by the nonlinear, large increase (6×) in the number of Pd particles per rod on going from 1 to 3 h irradiation (1.3 Pd particles to 8.0 Pd particles, respectively). On the basis of the band edge position of the two different CdS- or CdSe-rich domains, light emitted by the 575 nm lamp is strongly absorbed by the CdSe-rich head (~650 nm absorption edge), but not by the CdS-rich tail (~500 nm absorption edge). Because Pd nanoparticles form not only on the head but also on the tail of the nanorods (Figure 9c), we infer excitons can travel unimpeded across whole $CdS_{1-x}Se_x$ graded-alloy nanocrystals. In other words, exciton quenching by surface defects appears to occur at any point on the surface of these nanorods, leading to photoreduction of the Pd molecular precursor and surface seeding of Pd nanoparticles along the whole length of $CdS_{0.42}Se_{0.58}$ nanorods. A full detailed account on metal photodeposition behavior, characterization, and application of the resulting nanostructures will be the subject of a separate article.

CONCLUSIONS

In summary, we have prepared axially anisotropic $CdS_{1-x}Se_x$ nanorods *via* a single injection of a mixture of TOPS and TOPSe precursors to a hot cadmium−phosphonate complex. The morphology of the resulting nanocrystals strongly depends on relative amounts of S and Se used. Axially anisotropic nanorods with a thick head segment and a thin tail segment are obtained when the Se loading is between 5% and 10% of total chalcogenides. The aspect ratio of the nanorods decreases as Se loading increases. The optical properties of the nanostructures are tunable with composition. The absorption band edge of these nanostructures red shifts with increasing Se loading. X-ray diffraction and elemental analyses show that the actual Se content in $CdS_{1-x}Se_x$ nanorods is consistently higher than synthetic Se loading. X-ray diffraction data, Vegard's plots, and high-resolution TEM studies confirm that axially anisotropic nanorods possess a graded-alloy structure. Elemental mapping by energy-dispersive spectroscopy and energy-filtered TEM showed the head region of anisotropic nanorods is rich with Se and the tail region is rich with S. Time-dependent evolution studies show that the formation of these nanorods starts with homogeneous nucleation and quick growth of a thick CdSe-rich head, followed by heterogeneous nucleation and slow growth of a CdS-rich thin tail. This anisotropic growth can be attributed to the stability of chalcogenide precursors. TOPSe is less stable and more reactive compared to TOPS. As a result, TOPSe reacts with cadmium−phosphonate much faster, forming the head segment first. Over time, TOPS slowly reacts with cadmium−phosphonate, forming the thin tail segment along the *c* axis. Mechanistic experiments show the opposite synthetic sequence is not possible. Namely, formation of a CdSe-rich head does not occur starting from a CdS-rich tail. Metal deposition experiments conducted using 575 nm light irradiation show there is good electronic communication between the CdS-rich and CdSe-rich segments. We are currently exploring using axially anisotropic $CdS_{1-x}Se_x$ nanorods and $CdS_{1-x}Se_x$−Pd heterostructures as building blocks for more complex nanostructures and devices.

METHODS

Materials. Cadmium oxide (99.998%) and sulfur (99.999%) were purchased from AlfaAesar, octadecylphosphonic acid was from PCI Synthesis, selenium (99.999%), trioctylphosphine oxide (TOPO) (99%), triethylamine (≥99.5%), and anhydrous toluene were from Sigma-Aldrich, and trioctylphosphine (TOP) (97%) and *cis*-dimethyl(*N*,*N*,*N*′,*N*′-tetramethylethylenediamine)-palladium(II) ((TMEDA)$PdMe_2$) (99%) were from Strem. Materials

were used as received unless specified otherwise. CdS nanorods (154.1 ± 30.4 nm length, 5.6 ± 0.8 nm diameter) were prepared according to a literature procedure.[9] Elemental analyses were performed by Galbraith Laboratories, Inc., Knoxville, TN.

Synthesis of $CdS_{1-x}Se_x$ Nanorods. *TOP-Chalcogen Stock Solutions.* A solution of S (407.7 mg, 12.5 mmol) in TOP (4.61 g, 12.5 mmol) (2.25 M TOPS stock solution) and a solution of Se (987.0 mg, 12.5 mmol) in TOP (4.61 g, 12.5 mmol) (2.25 M TOPSe stock solution) were prepared under a dry N_2 atmosphere inside a glovebox. TOPS and TOPSe solutions were mixed in varying ratios to make different injection solutions (2.25 M TOP-chalcogen). *General synthesis procedure:* CdO (105.0 mg, 0.810 mmol), TOPO (1.375 g, 3.56 mmol), and ODPA (535 mg, 0.937 mmol) were weighed into a three-neck round-bottom (RB) flask. The flask was fitted with a glass-coated stir bar, a condenser, and a stainless steel thermocouple. The apparatus was sealed and brought onto an Schlenk line. Using a heating mantle, the mixture was heated to 100 °C, evacuated under vacuum for 15 min, refilled with argon, and heated to 320 °C to form a completely colorless solution. The solution was cooled to 120 °C, evacuated under vacuum for 15 min, refilled with argon, and heated back to 320 °C. When the temperature reached 300 °C, TOP (1.20 mL, 2.69 mmol) was injected into the flask. When the temperature reached 320 °C, a mixture of TOPS and TOPSe (1 mL total volume, 2.25 mmol total chalcogens) was rapidly injected, causing a gradual color change. Upon injection, the temperature was allowed to equilibrate at 315 °C and kept constant for a total reaction time of 85 min. The final reaction mixture was removed from the heating mantle and cooled to room temperature. After dilution with toluene (5 mL), nanocrystals were isolated by addition of a 1:1 v/v 2-propanol/nonanoic acid mixture (24 mL), followed by centrifugation (5000 rpm for 10 min).

Mechanistic Experiments. *Time Evolution.* We used the general synthetic procedure above starting from CdO (105.0 mg, 0.810 mmol), TOPO (1.375 g, 3.56 mmol), ODPA (535 mg, 0.937 mmol), and TOP (1.20 mL, 2.69 mmol), using a mixture of TOPS (0.95 mL, 2.1375 mmol) and TOPSe (0.05 mL, 0.1125 mmol) as chalcogenide injection solution (5% Se loading). We repeated this procedure, stopping the reaction at different times by removing the heating mantle and cooling to room temperature. Products were isolated as described above. *Reaction of CdSe nanorods with Cd−phosphonate and TOPS:* We first prepared pure CdSe nanorods by the general synthetic procedure starting from CdO (105.0 mg, 0.810 mmol), TOPO (1.375 g, 3.56 mmol), ODPA (535 mg, 0.937 mmol), and TOP (1.20 mL, 2.69 mmol), and using TOPSe (1.00 mL, 2.25 mmol). The reaction was stopped after 85 min, and products were isolated as described in the general synthetic procedure above. Isolated CdSe nanorods were dissolved in toluene (3 mL) and transferred to a new three-neck RB flask, and the solvent was removed under vacuum. In a separate flask, CdO (105.0 mg, 0.810 mmol), TOPO (1.375 g, 3.56 mmol), and ODPA (535 mg, 0.937 mmol) were weighed, heated to 100 °C, evacuated under vacuum for 15 min, refilled with argon, and heated to 320 °C to form a completely colorless solution. The solution was allowed to cool to 120 °C, evacuated under vacuum for 15 min, refilled with argon, and transferred to the flask containing the CdSe nanorods *via* syringe. The mixture of Cd−phosphonate precursor and CdSe nanorods was heated to 320 °C. When the temperature reached 300 °C, TOP (1.20 mL, 2.69 mmol) was injected into the flask. When the temperature reached 320 °C, a solution of TOPS (1 mL, 2.25 mmol) was rapidly injected. Upon injection, the temperature was allowed to equilibrate at 315 °C and kept constant for a total reaction time of 85 min. Products were isolated as described above. *Reaction of CdS nanorods with TOPSe:* We first prepared pure CdS nanorods[9] by the general synthetic procedure above starting from CdO (105.0 mg, 0.810 mmol), TOPO (1.375 g, 3.56 mmol), ODPA (535 mg, 0.937 mmol), and TOP (1.20 mL, 2.69 mmol), and using TOPS (1.00 mL, 2.25 mmol). The reaction was stopped after 85 min, and products were isolated as described above. Isolated CdS nanorods were transferred to a three-neck RB flask containing TOPO (1.375 g, 3.56 mmol). The mixture was heated to 100 °C, evacuated for 15 min, refilled with argon, and heated to 320 °C. At this temperature a mixture containing TOP (1.2 mL, 3.56 mmol) and TOPSe (0.05 mL, 0.1125 mmol) was rapidly injected. The temperature was allowed to equilibrate at 315 °C and kept constant for a total reaction time of 85 min. Products were isolated as described above.

Synthesis of $CdS_{0.42}Se_{0.58}$−Pd Heterostructures. $CdS_{0.42}Se_{0.58}$ nanorods obtained with a 10% Se loading were dissolved and diluted in toluene to give an optical density (absorbance) of 1.3 at 630 nm. A 2.0 mL volume of this solution was degassed, refilled with dry argon, and stored in the dark for 12 h in a resealable Schlenk tube. Under a dry atmosphere, (TMEDA)-$PdMe_2$ (30.0 mg, 0.118 mmol) was dissolved in anhydrous toluene (1 mL), and the solution was added to a $CdS_{1-x}Se_x$ nanorod solution *via* syringe along with triethylamine (0.5 mL, used as terminal electron donor).[71] Deposition was carried out for 1−3 h photochemically at room temperature in a Rayonet photoreactor containing 16 side-on fluorescent lamps (575 nm/75 nm fwhm). Products were purified twice by precipation with methanol (30 mL) and centrifugation (5000 rpm for 10 min). All products could be redispersed in toluene.

Structural Characterization. *X-ray Diffraction.* Powder X-ray diffraction data were measured using Cu Kα radiation on a Scintag XDS-2000 diffractometer equipped with a theta−theta goniometer, a sealed-tube solid-state generator, and an air-cooled Kevex Psi Peltier silicon detector. *Transmission electron microscopy:* Transmission electron microscopy of samples was conducted on carbon-coated copper grids using a FEI Technai G2 F20 field emission scanning transmission electron microscope (STEM) at 200 kV (point-to-point resolution <0.25 nm, line-to-line resolution <0.10 nm). Nanorods' elemental axial composition was characterized by energy-dispersive spectroscopy line scans in STEM mode and by energy-filtered imaging spectroscopy. *Particle analysis:* Dimensions were measured manually and/or by using ImageJ. Size measurements and particle counts/statistics were obtained for at least >50−100 $CdS_{1-x}Se_x$ and Pd particles. Average sizes are reported along with standard deviations. For axially anisotropic nanorods, we report two diameters: "head" diameter is the largest observed diameter; "tail" diameter is midpoint on the thinner half of the nanorods.

Optical Characterization. Absorption spectra were measured with a photodiode-array Agilent 8453 UV−vis spectrophotometer. Solvent absorption was recorded and subtracted from all spectra. Steady-state photoluminescence (PL) spectra were measured with a Horiba-Jobin Yvon Nanolog scanning spectrofluorometer equipped with a photomultiplier detector. Photoluminescence quantum yields (QYs) were measured following literature procedures.[80] Nanorod samples were diluted in hexane or toluene to give an optical density of 0.05−0.2 at 510 nm. Their PL emission was compared to rhodamine 590 in methanol, with QY = 95%. Excitation wavelength was 510 nm, and emission was recorded between 525 and 800 nm. QYs were calculated as follows: $QY_{QD} = 0.95 \times (OD_{rhodamine590}/OD_{QD}) \times (PLarea_{QD}/PLarea_{rhodamine590}) \times (RI_{QD}^2/RI_{rhodamine590}^2)$, where $RI_{rhodamine590}$ was taken as the refractive index of methanol (1.3288), and RI_{QD} as the refractive index of toluene (1.4941). Absorption and PL emission spectra of QD and dye samples were measured at least twice, and average QYs recorded.

Acknowledgment. This research was supported by the U.S. Department of Energy, Office of Basic Energy Sciences, Division of Chemical Sciences, Geosciences, and Biosciences, through the Ames Laboratory. The Ames Laboratory is operated for the U.S. Department of Energy by Iowa State University under Contract No. DE-AC02-07CH11358. We thank Iowa State University, the U.S. Department of Energy Ames Laboratory Royalty Account, and the Institute for Physical Research and Technology (IPRT) for laboratory startup funds (J.V.), Yijun Guo for assistance with PL measurements, and John Corbett and Gordie Miller for helpful discussions.

Supporting Information Available: Mechanistic, TEM, EDS, and XRD data. This material is available free of charge *via* the Internet at http://pubs.acs.org.

REFERENCES AND NOTES

1. Talapin, D. V.; Lee, J.-S.; Kovalenko, M. V.; Shevchenko, E. V. Prospects of Colloidal Nanocrystals for Electronic and Optoelectronic Applications. *Chem. Rev.* **2010**, *110*, 389–458.

2. Hochbaum, A. I.; Yang, P. Semiconductor Nanowires for Energy Conversion. *Chem. Rev.* **2010**, *110*, 527–546.
3. Wang, F.; Dong, A.; Sun, J.; Tang, R.; Yu, H.; Buhro, W. E. Solution-Liquid-Solid Growth of Semiconductor Nanowires. *Inorg. Chem.* **2006**, *45*, 7511–7521.
4. Kuno, M. An Overview of Solution-Based Semiconductor Nanowires: Synthesis and Optical Studies. *Phys. Chem. Chem. Phys.* **2008**, *10*, 620–639.
5. Hu, J.; Odoc, T. W.; Lieber, C. M. Chemistry and Physics in One Dimension: Synthesis and Properties of Nanowires and Nanotubes. *Acc. Chem. Res.* **1999**, *32*, 435–445.
6. Lu, W.; Lieber, C. M. Semiconductor Nanowires. *J. Phys. D: Appl. Phys.* **2006**, *39*, R387–R406.
7. Fan, H. J.; Werner, P.; Zacharias, M. Semiconductor Nanowires: From Self-Organization to Patterned Growth. *Small* **2006**, *2*, 700–717.
8. Peng, X. G.; Manna, L.; Yang, W. D.; Wickham, J.; Scher, E.; Kadavanich, A.; Alivisatos, A. P. Shape Control of CdSe Nanocrystals. *Nature* **2000**, *404*, 59–61.
9. Robinson, R. D.; Sadtler, B.; Demkencho, D. O.; Erdonmez, C. K.; Alivisatos, A. P. Spontaneous Superlattice Formation in Nanorods Through Partial Cation Exchange. *Science* **2007**, *317*, 355–358.
10. Sadtler, B.; Demchenko, D. O.; Zheng, H.; Hughes, S. M.; Merkle, M. G.; Dahmen, U.; Wang, L. W.; Alivisatos, A. P. Selective Facet Reactivity during Cation Exchange in Cadmium Sulfide Nanorods. *J. Am. Chem. Soc.* **2009**, *131*, 5285–5293.
11. Peng, Z. A.; Peng, X. Formation of High-Quality CdTe, CdSe, and CdS Nanocrystals Using CdO as Precursor. *J. Am. Chem. Soc.* **2001**, *123*, 183–184.
12. Jun, Y.; Lee, S.; Kang, N.; Cheon, J. Controlled Synthesis of Multi-armed CdS Nanorod Architectures Using Monosurfactant System. *J. Am. Chem. Soc.* **2001**, *123*, 5150–5151.
13. Saunders, A. E.; Ghezelbash, A.; Sood, P.; Korgel, B. A. Synthesis of High Aspect Ratio Quantum-Size CdS Nanorods and Their Surface-Dependent Photoluminescence. *Langmuir* **2008**, *24*, 9043–9049.
14. Sapra, S.; Poppe, J.; Eychmüller., A. CdSe Nanorod Synthesis: A New Approach. *Small* **2007**, *3*, 1186–1888.
15. Peng, Z. A.; Peng, X. Nearly Monodisperse and Shape-Controlled CdSe Nanocrystals via Alternative Routes: Nucleation and Growth. *J. Am. Chem. Soc.* **2002**, *124*, 3343–3353.
16. Felice, S.; Saunders, A. E.; Korgel, B. A. General Shape Control of Colloidal CdS, CdSe, CdTe Quantum Rods and Quantum Rod Heterostructures. *J. Phys. Chem. B* **2005**, *109*, 8539–8542.
17. Manna, L.; Scher, E. C.; Alivisatos, A. P. Synthesis of Soluble and Processable Rod-, Arrow-, Teardrop-, and Tetrapod-Shaped CdSe Nanocrystals. *J. Am. Chem. Soc.* **2000**, *122*, 12700–12706.
18. Huang, J.; Kovalenko, M. V.; Talapin, D. V. Alkyl Chains of Surface Ligands Affect Polytypism of CdSe Nanocrystals and Play an Important Role in the Synthesis of Anisotropic Nanoheterostructures. *J. Am. Chem. Soc.* **2010**, *132*, 15866–15868.
19. Wang, W.; Banerjee, S.; Jia, S.; Steigerwald, M. L.; Herman, I. P. Ligand Control of Growth, Morphology, and Capping Structure of Colloidal CdSe Nanorods. *Chem. Mater.* **2007**, *19*, 2573–2580.
20. Manna, L.; Wang, L. W.; Cingolani, R.; Alivisatos, A. P. First-Principles Modeling of Unpassivated and Surfactant-Passivated Bulk Facets of Wurtzite CdSe: A Model System for Studying the Anisotropic Growth of CdSe Nanocrystals. *J. Phys. Chem. B* **2005**, *109*, 6183–6192.
21. Peng, X. A.; Peng, X. Mechanisms of the Shape Evolution of CdSe Nanocrystals. *J. Am. Chem. Soc.* **2001**, *123*, 1389–1395.
22. Talapin, D. V.; Shevchenko, E. V.; Murray, C. B.; Kornowski, A.; Förster, S.; Weller, H. CdSe and CdSe/CdS Nanorod Solids. *J. Am. Chem. Soc.* **2004**, *126*, 12984–12988.
23. Li, L.-S.; Alivisatos, A. P. Origin and Scaling of the Permanent Dipole Moment in CdSe Nanorods. *Phys. Rev. Lett.* **2003**, *90*, 097402-1–097402-4.
24. Blanton, S. A.; Leheny, R. L.; Hines, M. A.; Guyot-Sionnest, P. Dielectric Dispersion Measurements of CdSe Nanocrystal Colloids: Observation of a Permanent Dipole Moment. *Phys. Rev. Lett.* **1997**, *79*, 865–868.
25. Swafford, L. A.; Weigand, L. A.; Bowers, M. J., II; McBride, J. R.; Rapaport, J. L.; Watt, T. L.; Dixit, S. K.; Feldman, L. C.; Rosenthal, S. J. Homogeneously Alloyed CdS_xSe_{1-x} Nanocrystals: Synthesis, Characterization, and Composition/Size-Dependent Band Gap. *J. Am. Chem. Soc.* **2006**, *128*, 12299–12306.
26. Zou, Y.; Li, D.; Yang, D. Noninjection Synthesis of CdS and Alloyed CdS_xSe_{1-x} Nanocrystals Without Nucleation Initiators. *Nanoscale Res. Lett.* **2010**, *5*, 966–971.
27. Ouyang, J.; Vincent, M.; Kingston, D.; Descours, P.; Boivineau, T.; Zaman, M. B.; Wu, X.; Yu, K. Noninjection, One-Pot Synthesis of Photoluminescent Colloidal Homogeneously Alloyed CdSeS Quantum Dots. *J. Phys. Chem. C* **2009**, *113*, 5193–5200.
28. Jang, E.; Jun, S.; Pu, L. High Quality CdSeS Nanocrystals Synthesized by Facile Single Injection Process and their Electroluminescence. *Chem. Commun.* **2003**, 2964–2965.
29. Bailey, R. E.; Nie, S. Alloyed Semiconductor Quantum Dots: Tuning the Optical Properties without Changing the Particle Size. *J. Am. Chem. Soc.* **2003**, *125*, 7100–7106.
30. Smith, A. M.; Nie, S. Bright and Compact Alloyed Quantum Dots with Broadly Tunable Near-Infrared Absorption and Fluorescence Spectra through Mercury Cation Exchange. *J. Am. Chem. Soc.* **2011**, *133*, 24–26.
31. Van Embden, J.; Jasieniak, J.; Mulvaney, P. Mapping the Optical Properties of CdSe/CdS Heterostructure Nanocrystals: The Effects of Core Size and Shell Thickness. *J. Am. Chem. Soc.* **2009**, *131*, 14299–14309.
32. Li, J. J.; Wang, Y. A.; Guo, W.; Keay, J. C.; Mishima, T. D.; Johnson, M. B.; Peng, X. Large-Scale Synthesis of Nearly Monodisperse CdSe/CdS Core/Shell Nanocrystals Using Air-Stable Reagents via Successive Ion Layer Adsorption and Reaction. *J. Am. Chem. Soc.* **2003**, *125*, 12567–12575.
33. Mahler, B.; Lequeux, N.; Dubertret, B. Ligand-Controlled Polytypism of Thick-Shell CdSe/CdS Nanocrystals. *J. Am. Chem. Soc.* **2010**, *132*, 953–959.
34. Vela, J.; Htoon, H.; Chen, Y.; Park, Y.-S.; Ghosh, Y.; Goodwin, P.; Werner, J.; Wells, N. P.; Casson, J. L.; Hollingsworth, J. A. Effect of Shell Thickness and Composition on Blinking Suppression and the Blinking Mechanism in `Giant' CdSe/CdS Nanocrystal Quantum Dots. *J. Biophoton.* **2010**, *3*, 706–717.
35. Bao, H.; Gong, Y.; Li, Z.; Gao, M. Enhancement Effect of Illumination on the Photoluminescence of Water-Soluble CdTe Nanocrystals: Toward Highly Fluorescent CdTe/CdS Core–Shell Structure. *Chem. Mater.* **2004**, *16*, 3853–3859.
36. Smith, A. M.; Mohs, A. M.; Nie, S. Tuning the Optical and Electronic Properties of Colloidal Nanocrystals by Lattice Strain. *Nature Nanotechnol.* **2009**, *4*, 56–63.
37. Dabbousi, B. O.; Rodriguez-Viejo, J.; Mikulec, F. V.; Heine, J. R.; Mattoussi, H.; Ober, R.; Jensen, K. F.; Bawendi, M. G. CdSe)ZnS Core–Shell Quantum Dots: Synthesis and Characterization of a Size Series of Highly Luminescent Nanocrystallites. *J. Phys. Chem.* **1997**, *101*, 9463–9475.
38. Talapin, D. V.; Rogach, A. L.; Kornowski, A.; Haase, M.; Weller, H. Highly Luminescent Monodisperse CdSe and CdSe/ZnS Nanocrystals Synthesized in a Hexadecylamine–Trioctylphosphine Oxide–Trioctylphospine Mixture. *Nano Lett.* **2001**, *1*, 207–211.
39. Malik, M. A.; O'Brien, P.; Revaprasadu, N. Simple Route to the Synthesis of Core/Shell Nanoparticles of Chalcogenides. *Chem. Mater.* **2002**, *14*, 2004–2010.
40. Hines, M. A.; Guyot-Sionnest, P. Synthesis and Characterization of Strongly Luminescing ZnS-Capped CdSe Nanocrystals. *J. Phys. Chem.* **1996**, *100*, 468–471.
41. Reiss, P.; Bleuse, J; Pron, A. Highly Luminescent CdSe/ZnSe Core/Shell Nanocrystals of Low Size Dispersion. *Nano Lett.* **2002**, *2*, 781–784.
42. Xie, R.; Kolb, U.; Li, J.; Basché, T.; Mews, A. Synthesis and Characterization of Highly Luminescent CdSe–Core CdS/$Zn_{0.5}Cd_{0.5}S$/ZnS Multishell Nanocrystals. *J. Am. Chem. Soc.* **2005**, *127*, 7480–7488.

43. Carbone, L.; Nobile, C.; De Giorgi, M.; Della Sala, F.; Morello, G.; Pompa, P.; Hytch, M.; Snoeck, E.; Fiore, A.; Franchini, I. R.; *et al*. Synthesis and Micrometer-Scale Assembly of Colloidal CdSe/CdS Nanorods Prepared by a Seeded Growth Approach. *Nano Lett.* **2007**, *7*, 2942–2950.
44. Zou, Y.; Li, D.; Yang, D. Single Step Synthesis of CdSeS Nanorods with Chemical Composition Gradients. *J. Cryst. Growth* **2010**, *312*, 3406–3409.
45. Talapin, D. V.; Nelson, J. H.; Shevchenko, E. V.; Aloni, S.; Sadtler, B.; Alivisatos, A. P. Seeded Growth of Highly Luminescent CdSe/CdS Nanoheterostructures with Rod and Tetrapod Morphologies. *Nano Lett.* **2007**, *7*, 2951–2959.
46. Gross, D.; Susha, A. S.; Klar, T. A.; Da Como, E.; Rogach, A. L.; Feldmann, J. Charge Separation in Type II Tunneling Structures of Close-packed CdTe and CdSe Nanocrystals. *Nano Lett.* **2008**, *8*, 1482–1485.
47. Halpert, J. E.; Porter, V. J.; Zimmer, J. P.; Bawendi, M. G. Synthesis of CdSe/CdTe Nanobarbells. *J. Am. Chem. Soc.* **2006**, *128*, 12590–12591.
48. McBride, J.; Treadway, J.; Feldman, L. C.; Pennycook, S. J.; Rosenthal, S. J. Structural Basis for Near Unity Quantum Yield Core/Shell Nanostructures. *Nano Lett.* **2006**, *6*, 1496–1451.
49. Koo, B.; Korgel, B. A. Coalescence and Interface Diffusion in Linear CdTe/CdSe/CdTe Heterojunction Nanorods. *Nano Lett.* **2008**, *8*, 2490–2496.
50. Tang, B.; Yang, F.; Lin, Y.; Zhuo, L.; Ge, J.; Cao, L. Synthesis and Characterization of Wavelength-Tunable, Water-Soluble, and Near-Infrared-Emitting CdHgTe Nanorods. *Chem. Mater.* **2007**, *19*, 1212–1214.
51. Liang, Y.; Zhai, L.; Zhao, X.; Xu, D. Band-Gap Engineering of Semiconductor Nanowires through Composition Modulation. *J. Phys. Chem. B* **2005**, *109*, 7120–7123.
52. Pan, A.; Yang, H.; Liu, R.; Yu, R.; Zou, B.; Wang, Z. Color-Tunable Photoluminescence of Alloyed CdS_xSe_{1-x} Nanobelts. *J. Am. Chem. Soc.* **2005**, *127*, 15692–15693.
53. Ouyang, L.; Maher, K. N.; Yu, C. L.; McCarty, J.; Park, H. Catalyst-Assisted Solution−Liquid−Solid Synthesis of CdS/CdSe Nanorod Heterostructures. *J. Am. Chem. Soc.* **2007**, *129*, 133–138.
54. Dong, A.; Tang, R.; Buhro, W. E. Solution-Based Growth and Structural Characterization of Homo- and Heterobranched Semiconductor Nanowires. *J. Am. Chem. Soc.* **2007**, *129*, 12254–12262.
55. Zhong, H.; Scholes, G. D. Shape Tuning of Type II CdTe-CdSe Colloidal Nanocrystal Heterostructures through Seeded Growth. *J. Am. Chem. Soc.* **2009**, *131*, 9170–9171.
56. Li, Y.; Zhong, H.; Li, R.; Zhou, Y.; Yang, Z.; Li, Y. High-Yield Fabrication and Electrochemical Characterization of Tetrapodal CdSe, CdTe, and $CdSe_xTe_{1-x}$ Nanocrystals. *Adv. Funct. Mater.* **2006**, *16*, 1705–1716.
57. Peng, X. Mechanisms for the Shape-Control and Shape-Evolution of Colloidal Semiconductor Nanocrystals. *Adv. Mater.* **2003**, *15*, 459–463.
58. Gunlach, L.; Piotrowiak, P. Ultrafast Spatially Resolved Carrier Dynamics in Single CdSSe Nanobelts. *J. Phys. Chem. C* **2009**, *113*, 12162–12166.
59. Joo, J.; Son, J. S.; Kwon, S. G.; Yu, J. H.; Hyeon, T. Low-Temperature Solution-Phase Synthesis of Quantum Well Structured CdSe Nanoribbons. *J. Am. Chem. Soc.* **2006**, *128*), 5632–5633.
60. Pacholski, C.; Kornowski, A.; Weller, H. Site-Specific Photodeposition of Silver on ZnO Nanorods. *Angew. Chem., Int. Ed.* **2004**, *43*, 4774–4777.
61. Costi, R.; Saunders, A. E.; Banin, U. Colloidal Hybrid Nanostructures: A New Type of Functional Materials. *Angew. Chem., Int. Ed.* **2010**, *49*, 4878–4897.
62. Habas, S. E.; Yang, P.; Mokari, T. Selective Growth of Metal and Binary Metal Tips on CdS Nanorods. *J. Am. Chem. Soc.* **2008**, *130*, 3294–3295.
63. Chan, S. C.; Barteau, M. A. Preparation of Highly Uniform Ag/TiO_2 and Au/TiO_2 Supported Nanoparticle Catalysts by Photodeposition. *Langmuir* **2005**, *21*, 5588–5595.
64. Kudera, S.; Carbone, L.; Casula, M. F.; Cingolani, R.; Falqui, A.; Snoeck, E.; Parak, W. J.; Manna, L. Selective Growth of PbSe on One or Both Tips of Colloidal Semiconductor Nanorods. *Nano Lett.* **2005**, *5*, 445–449.
65. Kwon, K.-W.; Lee, B. H.; Shim, M. Structural Evolution in Metal Oxide/Semiconductor Colloidal Nanocrystal Heterostructures. *Chem. Mater.* **2006**, *18*, 6357–6363.
66. Kwon, K.-W.; Shim, M. γ-Fe_2O_3/II−VI Sulfide Nanocrystal Heterojunctions. *J. Am. Chem. Soc.* **2005**, *127*, 10269–10257.
67. Gao, J.; Zhang, B.; Gao, Y.; Pan, Y.; Zhang, X.; Xu, B. Fluorescent Magnetic Nanocrystals by Sequential Addition of Reagents in a One-Pot Reaction: A Simple Preparation for Multifunctional Nanostructures. *J. Am. Chem. Soc.* **2007**, *129*, 11928–11935.
68. Menagen, G.; Macdonald, J. E.; Shemesh, Y.; Popov, I.; Banin, U. Au Growth on Semiconductor Nanorods: Photoinduced versus Thermal Growth Mechanisms. *J. Am. Chem. Soc.* **2009**, *131*, 17406–17411.
69. Chakrabortty, S.; Yang, J. A.; Tan, Y. M.; Mishra, N.; Chan, Y. Asymmetric Dumbbells from Selective Deposition of Metals on Seeded Semiconductor Nanorods. *Angew. Chem., Int. Ed.* **2010**, *49*, 1–6.
70. Elmalem, E.; Saunders, A. E.; Costi, R.; Salant, A.; Banin, U. Growth of Photocatalytic CdSe-Pt Nanorods and Nanonets. *Adv. Mater.* **2008**, *20*, 4312–4317.
71. Dukovic, G.; Merkle, M. G.; Nelson, J. H.; Hughes, S. M.; Alivisatos, A. P. Photodeposition of Pt on Colloidal CdS and CdSe/CdS Semiconductor Nanostructures. *Adv. Mater.* **2008**, *20*, 4306–4311.
72. Cozzoli, P. D.; Pellegrino, T.; Manna, L. Synthesis, Properties and Perspectives of Hybrid Nanocrystal Structures. *Chem. Soc. Rev.* **2006**, *35*, 1195–1208.
73. Shi, W.; Sahoo, Y.; Zeng, H.; Ding, Y.; Swihart, M. T.; Prasad, P. N. Anisotropic Growth of PbSe Nanocrystals on $Au\text{-}Fe_3O_4$ Hybrid Nanoparticles. *Adv. Mater.* **2006**, *18*, 1889–1894.
74. Shemesh, Y.; Macdonald, J. E.; Menagen, G.; Banin, U. Synthesis and Photocatalytic Properties of a Family of CdS-PdX Hybrid Nanoparticles. *Angew. Chem., Int. Ed.* **2011**, *50*, 1185–1189.
75. Maynadié, J.; Salant, A.; Falqui, A.; Respaud, M.; Shaviv, E.; Banin, U.; Soulantica, K.; Chaudret, B. Cobalt Growth on the Tips of CdSe Nanorods. *Angew. Chem., Int. Ed.* **2009**, *48*, 1814–1817.
76. Deka, S.; Falqui, A.; Bertoni, G.; Sangregorio, C.; Poneti, G.; Morello, G.; De Giorgi, M.; Giannini, C.; Cingolani, C.; Manna, L.; *et al*. Fluorescent Asymmetrically Cobalt-Tipped CdSe@CdS Core@Shell Nanorod Heterostructures Exhibiting Room-Temperature Ferromagnetic Behavior. *J. Am. Chem. Soc.* **2009**, *131*, 12817–12828.
77. Vegard, L. X-Rays in the Service of Research on Matter. *Z. Krystallogr.* **1928**, *67*, 239–259.
78. Xu, F.; Rock, P. A.; Ma, X.; Kauzlarich, S. M.; Navrotsky, A. Enthalpies of Formation of CdS_xSe_{1-x} Solid Solutions. *J. Mater. Res.* **2009**, *24*, 1368–1374.
79. McDonough, J. E.; Mendiratta, A.; Curley, J. J.; Fortman, G. C.; Fantasia, S.; Cummins, C. C.; Rybak-Akimova, E. V.; Nolan, S. P.; Hoff, C. D. Thermodynamic, Kinetic, and Computational Study of Heavier Chalcogen (S, Se, and Te) Terminal Multiple Bonds to Molybdenum, Carbon, and Phosphorus. *Inorg. Chem.* **2008**, *47*, 2133–2141.
80. Grabolle, M.; Spieles, M.; Lesnyak, V.; Gaponik, N.; Eychmüller, A.; Resch-Genger, U. Determination of the Fluorescence Quantum Yield of Quantum Dots: Suitable Procedures and Achievable Uncertainties. *Anal. Chem.* **2009**, *81*, 6285–6294.